Contribution from the Department of Chemistry,
Southern Methodist University, Dallas, Texas 75275

MNDO Calculations on *closo*-Stannacarboranes and Their Donor-Acceptor Complexes

John A. Maguire,* George P. Ford, and Narayan S. Hosmane

Received December 14, 1987

Structural distortions in a number of $SnC_2(R)_2B_4H_4$ (R = substituents on the cage carbons) (I) and $(C_{10}H_8N_2)SnC_2B_4H_6$ (II) complexes are studied by using MNDO-SCF molecular orbital calculations. The displacement of the Sn in I toward the unique boron on the C_2B_3 open face is shown to be the result of the various overlap interactions between the Sn and carborane orbitals and an increase in the carborane cage bonding. The increased displacement of the Sn towards the unique boron on complexation with $C_{10}H_8N_2$ to form II is caused by a weakening of the tin-C_{cage} bonding and the geometric requirements for maximizing tin-bipyridine bonding and minimizing ligand-ligand repulsion between the bipyridine and carborane ligands.

Introduction

The reactions of *nido*-carboranes with metal-containing compounds to produce *closo*- and *commo*-metallacarboranes have been extensively reported.[1,2] Most involve the incorporation of metal groups in the polyhedral structures of $C_2B_9H_{11}^{2-}$, $C_2B_4H_6^{2-}$, or their derivatives, to form the respective icosahedral and pentagonal-bipyramidal clusters. Because of the greater ease in obtaining samples suitable for single-crystal X-ray crystallography, most of the structural information is on the closo and commo transition-metal complexes of $C_2B_9H_{11}$. One of the more interesting structural features of these complexes is that the metal is not necessarily situated directly above the center of the pentagonal open face of the carborane but can be dislocated, or slipped, away from this centroidal position. The extent and direction of slippage depends on the metal group and the relative positions of the boron and carbon atoms in the carborane.[3] There have been a number of theoretical explanations proposed for these distortions.[4]

There has been very little theoretical work published on the pentagonal-bipyramidal metallacarboranes in which the capping group bonds through a main-group metal. Until quite recently, the only structure reported was that of *closo*-1-CH_3-1-Ga-2,3-$C_2B_4H_6$ by Grimes and co-workers.[5] The gallium is slipped toward the unique boron in the C_2B_3 face and the CH_3-Ga bond is tilted so that the CH_3 is above the carbon atoms of the ring. Canadell, Eisenstein, and Rubio explained the tilting of the CH_3-Ga bond in terms of an increased bonding interaction with the unique boron.[6] Hosmane and co-workers have reported the structures of the series *closo*-1-Sn-2-$SiMe_3$-3-R-2,3-$C_2B_4H_4$ (R = $SiMe_3$, CH_3, H).[7-9] These stannacarboranes all show that the Sn atom is slipped toward the unique boron in the C_2B_3 face.[2]

Table I. Calculated and Experimental Bond Distances (Å) for 1-Sn-2-[$SiMe_3$]-3-[R]-2,3-$C_2B_4H_4$

	R = CH_3[b]		R = $SiMe_3$[c]		R = H[d]	
bond	exptl	calcd	exptl	calcd	exptl	calcd
C(1)-C(2)	1.480	1.526	1.501	1.5435	1.490	1.517
C(2)-B(3)	1.547	1.579	1.585	1.590	1.59	1.568
B(3)-B(4)	1.678	1.676	1.678	1.663	1.65	1.685
B(6)-C(2)	1.729	1.806	1.724	1.808	1.73	1.814
B(6)-B(3)	1.774	1.827	1.772	1.820	1.77	1.828
B(6)-B(5)	1.742	1.814	1.763	1.816	1.75	1.828
B(6)-B(4)	1.734	1.789	1.759	1.812	1.74	1.783
Sn-C(1)	2.476	2.337	2.503	5.334	2.518	2.332
Sn-C(2)	2.489	2.334	2.492	3.309	2.475	2.325
Sn-B(3)	2.426	2.299	2.452	2.283	2.432	2.289
Sn-B(4)	2.378	2.293	2.425	2.313	2.397	2.293
Sn-B(5)	2.405	2.290	2.434	2.294	2.431	2.303
Si-C(1)	1.886	1.828	1.886	1.827	1.885	1.823
R-C(2)	1.489	1.557	1.87	1.827		

[a] See Figure 1 for numbering system. [b] Reference 1. [c] Reference 2. [d] Reference 3.

Upon complexation of the tin with 2,2'-bipyridine ($C_{10}H_8N_2$), the metal undergoes an increased slip distortion.[8,10] On the basis of Fenske-Hall SCF calculations on the model compound, (bpy)-$SnC_2(CH_3)_2B_4H_4$, Fehlner suggested that the slip distortion was caused by the need to relieve an antibonding interaction between the tin "lone pair" and the cage carbons of the carborane.[11] Since these calculations were not extended to $SnC_2(CH_3)_2B_4H_4$ itself, where the same type of slippage occurs, they provide limited insight into the precise role of the bipyridine ligand.

While calculations of this kind provide a convenient framework for qualitative discussion, they do not give quantitative geometric or energetic predictions. Thus, the relative importance of the different factors that ultimately determine these quantities cannot be assessed. We, therefore, decided to study several stannacarboranes of the type $Sn(C_2R_2B_4H_4)$ (R = substituent on the cage carbon) and their bipyridine adducts by using MNDO[12-16] semiempirical molecular orbital theory. Applications of MNDO to compounds comprising elements of the second row, including boron,[16-18] are well documented.[19] Here its performance appears to be comparable to that of split valence shell ab initio calculations

(1) (a) Grimes, R. N. In *Comprehensive Organometallic Chemistry*; Wilkinson, G., Stone, F. G. A., Abel, E. W., Eds.; Pergamon: Oxford, England, 1982; Vol. 1, Chapter 5.5 and references therein. (b) Grimes, R. N. In *Metal Interactions with Boron Clusters*; Grimes, R. N., Ed.; Plenum: New York, 1982; and references therein.
(2) Hosmane, N. S.; Maguire, J. A. In *Molecular Structure and Energetics*; Liebman, J. F., Greenberg, A., Williams, R. E., Eds.; VCH: New York, 1988; Vol. 5, Chapter 14, pp 297-328 and references therein.
(3) (a) Dunks, G. B.; Hawthorne, M. F. In *Boron Hydride Chemistry*; Muetterties, E. L., Ed.; Academic: New York, 1975, and references therein. (b) Barker, G. K.; Green, M.; Onak, T. P.; Stone, F. G. A.; Ungermann, C. B.; Welch, A. J. *J. Chem. Soc., Chem. Commun.* **1978**, 168 and references therein. (c) Colquhoun, H. M.; Greenough, T. J.; Wallbridge, M. G. H. *J. Chem. Soc., Dalton Trans.* **1985**, 761. (d) Green, M.; Howard, J. A. K.; James, A. P.; Jelfs, A. N. M.; Nunn, C. M.; Stone, F. G. A. *J. Chem. Soc., Chem. Commun.* **1985**, 1778.
(4) (a) Mingos, D. M. P.; Forsyth, M. I.; Welch, A. J. *J. Chem. Soc., Dalton Trans.* **1978**, 1363. (b) Calhorda, M. J.; Mingos, D. M. P.; Welch, A. J. *J. Organomet. Chem.* **1982**, 228, 309. (c) Mingos, D. M. P. *J. Chem. Soc., Dalton Trans.* **1977**, 602. (d) Mingos, D. M. P.; Forsyth, M. I.; Welch, A. J. *J. Chem. Soc., Chem. Commun.* **1977**, 605.
(5) Grimes, R. N.; Rademaker, W. J.; Denniston, M. L.; Bryan, R. F.; Greene, P. T. *J. Am. Chem. Soc.* **1972**, *94*, 1865.
(6) Candell, E.; Eisenstein, O.; Rubio, J. *Organometallics* **1984**, *3*, 759.
(7) Cowley, A. H.; Galow, P.; Hosmane, N. S.; Jutzi, P.; Norman, N. C. *J. Chem. Soc., Chem. Commun.* **1984**, 1564.
(8) Hosmane, N. S.; de Meester, P.; Maldar, N. N.; Potts, S. B.; Chu, S. S. C.; Herber, R. H. *Organometallics* **1986**, *5*, 772.
(9) Hosmane, N. S.; Potts, S. B.; Siriwardane, U.; Alexander, J. J.; Shore, S. G., to be submitted for publication.
(10) Siriwardane, U.; Hosmane, N. S.; Chu, S. S. C. *Acta Crystallogr., Sect. C: Cryst. Struct. Commun.* **1987**, *C43*, 1067.
(11) Barreto, R. D.; Fehlner, T. P.; Hosmane, N. S. *Inorg. Chem.* **1988**, *27*, 453.
(12) Dewar, M. J. S.; Thiel, W. *J. Am. Chem. Soc.* **1977**, *99*, 4899.
(13) Dewar, M. J. S.; Thiel, W. *J. Am. Chem. Soc.* **1977**, *99*, 4907.
(14) Dewar, M. J. S.; Friedheim, J.; Healy, E. F.; Stewart, J. J. P. *Organometallics* **1986**, *5*, 375.
(15) Dewar, M. J. S.; Grady, G. L.; Stewart, J. J. P. *J. Am. Chem. Soc.* **1984**, *106*, 6771.
(16) Dewar, M. J. S.; McKee, M. L. *J. Am. Chem. Soc.* **1977**, *99*, 5231.
(17) Dewar, M. J. S.; McKee, M. L. *Inorg. Chem.* **1980**, *19*, 2662.
(18) DeKock, R. L.; Fehlner, T. P.; Housecroft, C. E.; Zubben, T. V.; Wade, K. *Inorg. Chem.* **1982**, *21*, 25. Andersen, E. L.; DeKock, R. L.; Fehlner, T. P. *J. Am. Chem. Soc.* **1980**, *102*, 2644.
(19) For an index of MNDO calculations through 1984 see: Clark, T. In *A Handbook of Computational Chemistry. A Practical Guide to Chemical Structure and Energy Calculations*; Wiley: New York, 1985; pp 188-232.

0020-1669/88/1327-3354$01.50/0 © 1988 American Chemical Society

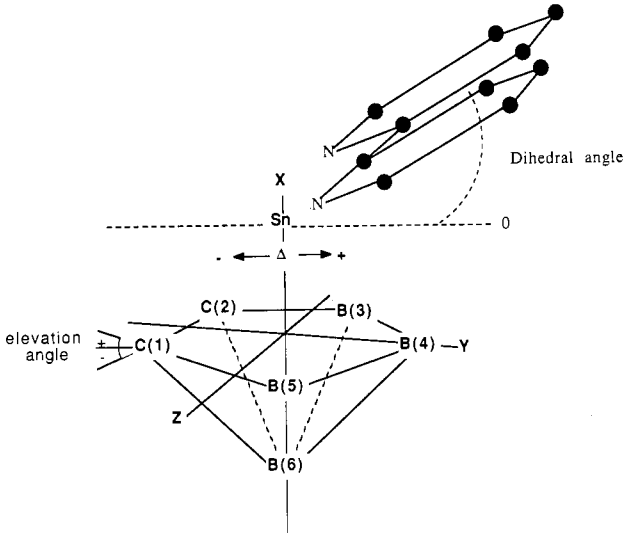

Figure 1. Atomic numbering system and geometric definitions for the stannacarboranes and their 2,2′-bipyridine complexes.

using modest basis sets.[20,21] MNDO performs less well for tin compounds.[15] However, a number of studies[22] using the recently announced tin parameters[15] seem to have provided useful results. We judged that such calculations on the stannaboranes should provide, at least, a semiquantitatively reliable understanding of the factors governing the precise location of the apical atom or group in molecules of this kind.

Calculations

All calculations were carried out by using Version[23] 2.10 of the MOPAC package[24] on an IBM 3081 running under the VM/CMS operating system. Unless noted otherwise, all geometrical variables were completely optimized with the modified[25] Davidon–Fletcher–Powell algorithm[26] incorporated as a standard program option. For calculations on molecules bearing the $SiMe_3$ group, we used the newer silicon parameters[14] rather than the earlier ones[27] despite the fact that the latter gave slightly better geometries and charge distributions more akin to those expected on electronegativity grounds.[14]

Results and Discussion

***closo*-1-$SnC_2(SiMe_3)RB_4H_4$.** Table I lists the experimental and calculated bond lengths for *closo*-$SnC_2(SiMe_3)(R)B_4H_4$ (R = $SiMe_3$, CH_3 and H). Experimentally, all structures show that the complexes have a pentagonal-bipyramidal geometry in which the Sn is slipped toward the unique boron, B(4), in Figure 1. The C_2B_3 face is not planar but is slightly folded such that the B(4) is about 0.05 Å below the C(1)–C(2)–B(3) plane, that is, displaced toward the apical boron, B(6) (see Figure 1 for orientation and numbering system). The substituents on the cage carbons are directed downward away from the Sn. For example, the elevation angle of the $SiMe_3$ is about −11.8° (see Figure 1). Although these distortions are small, they appear consistently and have been found to be related to slip distortion.[4a,28] The optimum structures

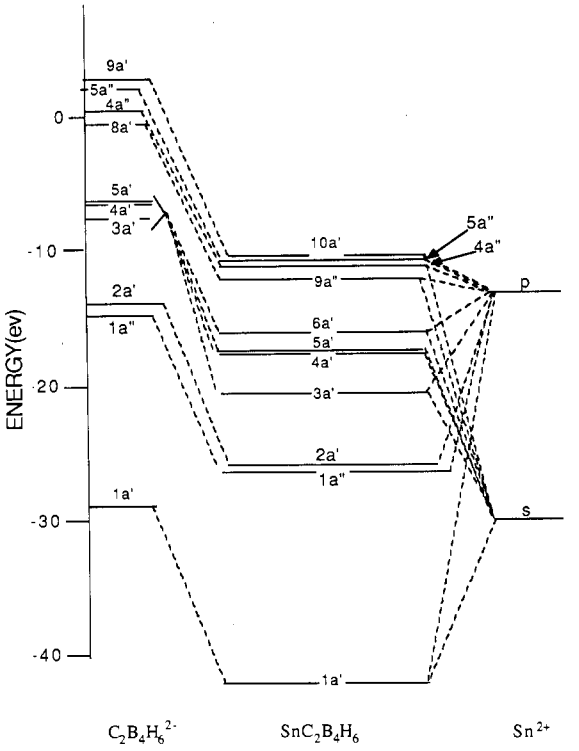

Figure 2. Partial molecular orbital correlation diagram for *closo*-$SnC_2B_4H_6$.

predicted by the MNDO calculations have these same general features, that is, a slippage of the Sn toward the unique boron, a folding of the C_2B_3 ring (about 0.02 Å), and a negative elevation angle of the $SiMe_3$ groups (−10.8°). As can be seen from Table I, MNDO tends to overestimate the bond distances involving the apical boron, B(6). Dewar and McKee[16] have reported MNDO calculations on a number of *closo*- and *nido*-carboranes and have found the same general behavior. MNDO tends to underestimate the energies of boron multicentered bonds compared to two-centered ones. Since the capping tin and the apical boron are competing for the same orbitals of the C_2B_3 ring, the underestimation of the apical boron interactions leads to an overestimation of the Sn–C_2B_3 interactions with the result that MNDO predicts Sn bond distances that are smaller than experimentally observed. Despite these differences, the experimental bonding trends seem to be well duplicated by the calculations.

Because of ring folding, a comparison of Sn–C_{cage} and Sn–B_{ring} distances cannot be used as a direct measure of the slippage of the metal. An alternative way of denoting the slip distortion is to measure the displacement, Δ, of the metal from the normal line connecting the C(1)–C(2)–B(3) plane and the apical boron, with a +Δ indicating slippage toward B(4) and a −Δ indicating slippage toward the cage carbons (see Figure 1). For comparison, the C–C cage bond is at Δ = −1.03; B(3)–B(5) is at Δ = 0.38, and B(4) is at Δ = 1.42. This is similar to the Δ defined by Mingos for the icosahedral metallacarborane systems.[4] Experimentally, the values of Δ for *closo*-$SnC_2(SiMe_3)(R)B_4H_4$ are 0.16, 0.8, and 0.21 for R = $SiMe_3$, CH_3, and H, respectively. The calculated values are 0.03, 0.10, and 0.07, respectively. When R = H, both experiment and calculations show that the Sn is displaced away from the side of the carborane containing the $SiMe_3$ group. (The displacements are as follows: found, 0.072 Å; calculated, 0.013 Å.)

***closo*-$SnC_2B_4H_6$.** In order to assess the relative importance of the factors directing the slippage of the tin, calculations were carried out on the model compound *closo*-$SnC_2B_4H_6$. Hydrogens were chosen as the substituents to minimize steric factors. The calculated optimum geometry showed a slippage of the tin atom toward B(4) (Δ = 0.04), a folded C_2B_3 face (B(4) depressed by 0.04 Å), and negative elevation angle of the cage carbon substituents (angle = −7.2°).

(20) Dewar, M. J. S.; Ford, G. P. *J. Am. Chem. Soc.* **1979**, *101*, 5558.
(21) Dewar, M. J. S.; Storch, D. M. *J. Am. Chem. Soc.* **1985**, *107*, 3898.
(22) Dewar, M. J. S.; Grady, G. L.; Kuhn, D. R.; Merz, Jr., K. M. *J. Am. Chem. Soc.* **1984**, *106*, 6773. Dewar, M. J. S.; Grady, G. L.; Kuhn, D. R. *Organometallics* **1985**, *4*, 1041. Dewar, M. J. S.; Grady, G. L. *Ibid.* **1985**, *4*, 1327.
(23) Olivella, S. *QCPE Bull.* **1984**, *4*, 109.
(24) Stewart, J. P. *QCPE Bull.* **1983**, *3*, 43.
(25) Weiner, P. K. Ph.D. Dissertation, University of Texas at Austin, 1975.
(26) Davidon, W. C. *Comput. J.* **1968**, *10*, 406. Fletcher, R.; Powell, M. J. D. *Ibid.* **1963**, *6*, 163.
(27) Dewar, M. J. S.; McKee, M. L.; Rzepa, H. S. *J. Am. Chem. Soc.* **1978**, *100*, 3607.
(28) Colquhoun, H. M.; Greenhough, T. J.; Wallbridge, M. G. H. *J. Chem. Soc., Chem. Commun.* **1976**, 1019; *Acta Crystallogr., Sect. B: Struct. Crystallogr. Cryst. Chem.* **1977**, *B33*, 3604.

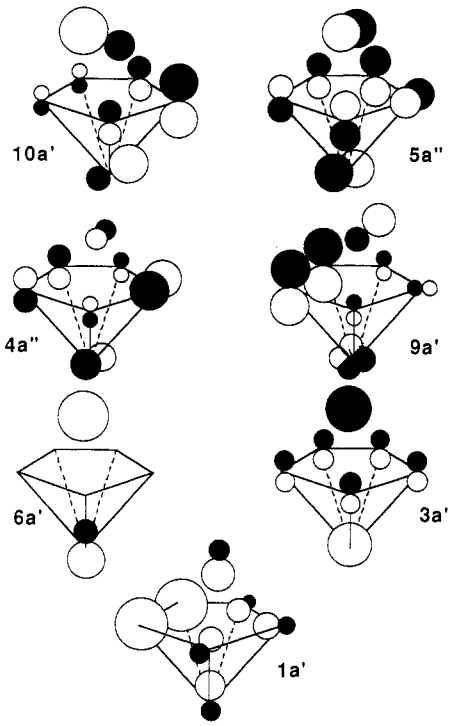

Figure 3. Atomic orbital composition sketches of some molecular orbitals of *closo*-$SnC_2B_4H_6$.

Both $C_2B_4H_6^{2-}$ and $SnC_2B_4H_6$ were assumed to possess C_s symmetry with a mirror plane containing B(4), B(6), and the midpoint of the C–C bond. The molecular orbitals (MO's) are either symmetric (a′) or antisymmetric (a″) to reflection in this plane. The $C_2B_4H_6^{2-}$ has 14 filled MO's, while $SnC_2B_4H_6$ has 15. Their molecular orbital configurations up through the highest occupied MO are 1a′1a″2a′3a′2a″4a′5a′6a′3a″7a′8a′4a″5a″9a′ and 1a′1a″2a′3a′2a″4a′5a′6a′7a′3a″8a′9a′4a″5a″10a′, respectively. The principal bonding interactions between the metal and the $C_2B_4H_6^{2-}$ moiety involve those orbitals of the latter extending above the C_2B_3 face. In the coordinate frame shown in Figure 1, these will be orbitals having appreciable p_x components. For the unmetalated dianion ($C_2B_4H_6^{2-}$) the MO's of interest are 3a′,8a′,4a″,5a″, and 9a′.[29] These interact with the tin valence orbitals of the appropriate symmetry. Here, the tin s, p_x, and p_y orbitals have a′ symmetry, and the p_z orbital has a″ symmetry. Figure 2 shows a partial molecular orbital correlation diagram for these interactions. The forms of some of the resulting orbitals in the stannaborane ($SnC_2B_4H_6$) are shown in Figure 3. The atomic orbital contributions of the non-hydrogen atoms in these MO's are given in Table 2S of the supplementary material.

The two highest energy MO's of $C_2B_4H_6^{2-}$, 5a″ and 9a′, are quite similar to the analogous carborane MO's calculated by Mingos for the icosahedral $MC_2B_9H_{11}$ systems.[4d] Because of the similar ligating properties of $C_2B_4H_6^{2-}$ and $C_2B_9H_{11}^{2-}$, it has generally been assumed that the two carboranes are using similar MO's when bonding to metals.[2] These similarities have been demonstrated by using arguments based on extended Hückel calculations[4b] and are also evident in the present work.

The $SnC_2B_4H_6$ MO's 3a′ and 6a′ are predominantly localized on the tin. Indeed, together the electrons associated with these orbitals account for 76.4% of the total Sn s-electron population and can be thought of as constituting its "lone pair" electrons. From the nearly symmetric electron distribution about the tin in these orbitals, it is not surprising that the tin in the stannacarboranes fails to act as a donor site in forming acid–base adducts.[30] On the contrary, it has been found experimentally that the tin acts as a Lewis acid site.[8,10] Mulliken overlap populations[31]

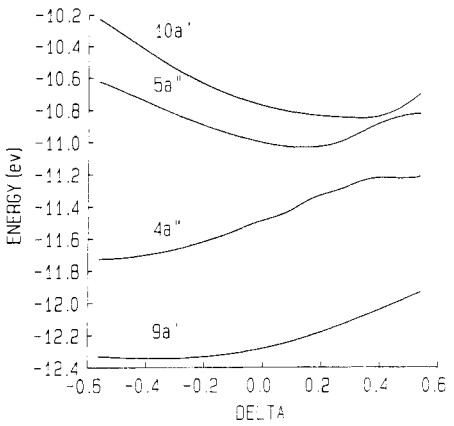

Figure 4. Energy of some molecular orbitals of *closo*-$SnC_2B_4H_6$ as a function of Δ.

Table II. Mulliken Charge Distributions

	charge			
	$[C_2B_4H_8]$	$[C_2B_4H_6]^{2-}$	$Sn[C_2B_4H_6]$	BP.Sn[$C_2B_4H_4$]
C(1)	0.009	−0.151	−0.115	−0.050
C(2)	0.009	−0.151	−0.115	−0.050
B(3)	−0.135	−0.223	−0.270	−0.318
B(4)	0.033	−0.277	−0.218	−0.340
B(5)	−0.135	−0.223	−0.270	−0.318
B(6)	−0.256	−0.342	−0.056	−0.090
Sn			0.680	0.692

also reflect this lack of Sn s orbital participation in bonding to the carborane. The overlap populations for the different tin interactions are Sn–C = 0.0136, Sn–B(4) = −0.0002, and Sn–B(3) = −0.0302. An analysis of the individual tin orbital contributions show that the Sn s orbitals make negative contributions to all populations; the shorter the bond distance to the tin, the more negative the contribution. Favorable bonding interactions are through the Sn p orbitals.

Calculations of the energies of MO's involving significant contributions from the Sn as a function of Δ show that, in general, those MO's localized on the borons (5a″ and 10a′) are stabilized by positive Δ's while the carbon centered ones (1a′, 9a′, and 4a″) are stabilized by negative Δ's. Molecular orbital 3a′, which has a nearly symmetric C_2B_3 distribution, has a broad energy minimum at Δ = 0; the energy of MO 6a′ is essentially independent of Δ. While changes in the individual orbital energies do not quantitatively parallel[33] changes in the total electronic energy of the system, their behavior as a function of the position of the tin is instructive (cf. Figure 4). The slippage of the Sn is along the nodal plane in MO 5a″. Since this orbital is localized more on B(3), B(5) than on C(1), C(2) (18.5% B(3) character vs 10.6% C(1) character), a slight slippage (Δ < 0.2) produces stability. However, as Δ increases beyond this value, its energy increases. The only interaction between the Sn p_z orbital and B(4) is through

(29) See supplementary Table 1s for the compositions of the MO's.
(30) Hosmane, N. S.; Sirmokadam, N. N.; Herber, R. H. *Organometallics* **1984**, *3*, 1665.
(31) A standard Mulliken population analysis[32] was carried out on the deorthogonalized MNDO eigenvectors; c.f.: Stewart, J. J. P. In "MOPAC Manual. A General Molecular Orbital Package", 2nd ed.; QCPE program 486; Quantum Chemistry Program Exchange: Bloomington, IN, 1984; pp 3–12.
(32) Mulliken, R. S. *J. Chem. Phys.* **1962**, *36*, 3428.
(33) At the Hartree-Fock level the electronic energy of a closed-shell molecule with n doubly occupied orbitals (ϵ_{tot}) is given by

$$\epsilon_{tot} = 2\sum_{i}^{n}\epsilon_i + \sum_{i}^{n}\sum_{j}^{n}(2J_{ij} - K_{ij})$$

where ϵ_i are the orbital energies and J_{ij} and K_{ij} are the coulomb and exchange integrals. Only in Hückel-type treatments, i.e. those in which electron repulsion integrals of the latter type are neglected, is the total energy simply the sum of the orbital energies. See for example: Pople, J. A.; Beveridge, D. In *Approximate Molecular Orbital Theory*; McGraw-Hill: New York, 1970; p 36.
(34) See supplementary Table 3S for calculated changes and Δ's for some substituted stannacarboranes.

Table III. One-Center and Two-Center Terms for $Sn(C_2B_4H_6)$ and $[Sn(B_6H_6)]^{2-}$ as a Function of Δ

			$Sn(C_2B_4H_6)$				
Δ,[a] Å	−0.552	−0.443	−0.336	0.084[b]	0.265	0.652	0.820
$\sum E_{AB}$(cage),[c] eV	−157.126	−157.489	−157.869	−159.351	−159.972	−161.158	−161.567
$\sum E_{AB}$(Sn–cage), eV	−20.042	−20.123	−20.158	−19.953	−19.685	−19.006	−18.753
E_A(Sn), eV	−83.840	−83.935	−83.998	−83.924	−83.744	−83.196	−82.952
$\sum E_A$(cage), eV	−454.180	−453.871	−453.590	−452.742	−452.501	−452.207	−452.127
E, eV	−715.188	−715.418	−715.615	−715.970	−715.902	−715.567	−715.399
			$[Sn(B_6H_6)]^{2-}$				
Δ, Å	−0.693	−0.513	−0.344	0[b]	0.301	0.654	1.072
$\sum E_{AB}$(cage), eV	−142.418	−142.953	−143.274	−143.546	−143.329	−142.575	−141.338
$\sum E_{AB}$(Sn–cage), eV	−23.503	−23.746	−24.020	−24.291	−24.102	−23.510	−22.582
E_A(Sn), eV	−85.654	−85.723	−85.774	−85.815	−85.776	−85.650	−85.476
$\sum E_A$(cage), eV	−350.223	−349.909	−349.691	−349.506	−349.639	−350.137	−351.071
E, eV	−601.798	−602.331	−602.759	−603.158	−602.846	−601.872	−600.467

[a] A positive Δ means displacement toward B(4). [b] Optimized value. [c] Cage = borane (B_6H_6) or carborane ($C_2B_4H_6$) cage.

the B(4) p_z orbital. Although the B(4) p_z does contribute to the MO, its interaction is much less than those of the p_x orbitals on the other atoms in the C_2B_3 face. Also ring folding will move this orbital farther away from the tin. At large Δ's there is considerable mixing of 4a″ and 5a″, which also tends to destabilize the latter and stabilize the former. The highest occupied MO, 10a′, which is localized on the ring borons with the B(4) p_x orbital making the largest contribution (26%), is also stabilized by small positive Δ's but increases in energy for larger values. The Sn s orbital is antibonding to the ring borons while the Sn p_x and Sn p_y orbitals are bonding. The Sn p_x interaction would be stabilized by a positive Δ; the greater the slippage, the greater the stability. However, such a slippage would increase the antibonding interaction of the Sn s. On the other hand, Sn p_y bonding would be enhanced by a small slippage but would rapidly become antibonding as Δ increased. Thus, the energy change of 10a′ is a result of these competing interactions.

Although the above discussion is useful in describing the changes in the different orbital interactions as Δ varies, it cannot be used to explain why slippage produces an overall energy lowering. Table II lists the Mulliken charges for $SnC_2B_4H_6$ and some related compounds. As can be seen from this table, although the electron density is greater on the cage carbons, it is not large enough to compensate for their higher nuclear charges and the boron atoms are more negative than the carbons. For the stannacarboranes, the borons on the C_2B_3 face bear most of the negative charge, which increases with increasing Δ. This polarization of electron density toward the boron side of the carborane face will affect not only the tin bonding but also bonding within the carborane moiety. In the MNDO approximation, the total energy of the molecule, E, can be expressed as the sum of one-center terms, E_A, and two-center terms, E_{AB}.[35-37]

$$E = \sum_A E_A + \sum_{A<B} \sum E_{AB}$$

E_{AB} has been found to provide a good quantitative measure of the A–B bond strength.[36] A large negative E_{AB} implies strong bonding while a positive value implies antibonding interactions. Table III lists, as a function of Δ, the one- and two-center terms for the different interactions in *closo*-$Sn(C_2B_4H_6)$ and, for comparison purposes, similar terms for the hypothetical *closo*-Sn-$(B_6H_6)^{2-}$. In these calculations the C_2B_4 cage was fixed at the average positions for the complexes shown in Table I, and the borane cage was fixed at its optimized geometry. As can be seen from the table, maximum Sn–cage bonding in $SnC_2B_4H_6$ does not coincide with the optimized value of Δ but rather at a position further removed toward the carbon atoms. For the symmetric stannaborane,[38] both maximum tin bonding and total stability occur when the tin is situated symmetrically above the open pentagonal face of the borane. Thus, the calculations show that the slippage of the tin is more a function of stabilizing internal carborane bonding rather than maximizing tin–carborane interactions. An analysis of the various contributing terms shows that more favorable B(6)–B(4), C(1/2)–B(3/5) and C(1)–C(2) interactions as Δ increases are primarily responsible for the increased cage bonding. When the $C_2B_4H_6$ cage bond distances were allowed to optimize, it was found that more positive values of Δ gave rise to an increase in ring folding and a shorter C_{cage}–C_{cage} bond distance. Both of these changes have been found to be related to metal slippage in the metallacarboranes.[4a,28]

The extent of slip distortion is the result of a number of interactions. The major tin covalent interactions favoring a positive Δ are found in 10a′, with Sn p_x bonding favoring slippage while Sn p_y and Sn p_z interactions tend to limit the extent of slippage. These are offset by similar interactions in 9a′ and 1a′ that favor a slippage toward the carbon atoms. In addition, the higher polarizability of the boron atoms would tend to favor slippage by increasing intracarborane bonding. Any change of the capping group that would favor greater involvement in carbon-centered orbitals, such as 1a′ and 9a′, as opposed to higher energy boron-based orbitals, such as 5a″ or 10a′, should limit slippage toward boron. Electron-withdrawing substituents on the cage carbons should enhance slippage toward boron by decreasing the carbon content in MO's 1a′ and 9a′ and by increasing B(6) bonding to the ring borons relative to the cage carbons. Unfortunately, experimental difficulties limit the extent to which these conclusions can be tested. Although *closo*-germacarboranes and *closo*-plumbacarboranes have been synthesized, no structural data are available.[1,2] There are at present no experimental studies of the effects of polyhedral substituents on slip distortion. However, Grimes has recently described some general routes for functionalized carbon and boron derivatives of *nido*-$C_2B_4H_8$.[39] Thus, it may be possible to obtain structural information on a series of metallacarboranes with a common capping group and varying ring substituents.

$(C_{10}H_8N_2)SnC_2B_4H_6$. Structural information is available on $(bpy)SnC_2(SiMe_3)(R)B_4H_4$ (R = $SiMe_3$ and CH_3).[8,10] A comparison of these compounds with their respective stannacarboranes shows that, on complexation with bipyridine, the tin is slipped more toward the boron side of the C_2B_3 face and the tin–carborane distance is increased. The bipyridine molecule is directly opposite the cage carbons, and the dihedral angles between the bipyridine rings and the C_2B_3 face are 18.4 and 26.8° for R = $SiMe_3$ and R = CH_3, respectively (see Figure 1). To ascertain what factors influence the increased slippage and the orientation of the bipyridine molecule, MNDO calculations were carried out on the model compound $(bpy)SnC_2B_4H_6$. Hydrogens were again chosen as the cage carbon substituents to minimize steric factors. A comparison of the optimized geometry of this compound with that

(35) Fisher, H.; Kollmar, H. *Theor. Chim Acta.* **1970**, *16*, 163.
(36) Dewar, M. J. S.; Lo, D. H. *J. Am. Chem. Soc.* **1971**, *93*, 7201.
(37) Olivella, S.; Vilarrusa, J. *J. Heterocycl. Chem.* **1981**, *18*, 1189.
(38) The $B_6H_6^{4-}$ ion can be formally considered to be formed by replacing the two cage carbons in $C_2B_4H_6^{2-}$ with B^- ions. The general numbering system shown in Figure 1 is still used; a positive value of Δ indicates movement of the tin in $[SnB_6H_6]^{2-}$ toward B(4) and away from B(1) and B(2).
(39) Grimes, R. N. Paper presented at the VIth International Meeting on Boron Chemistry, at Bechyne, Czechoslovakia, June 1987. Grimes, R. N. *Pure Appl. Chem.* **1987**, *59*, 847.

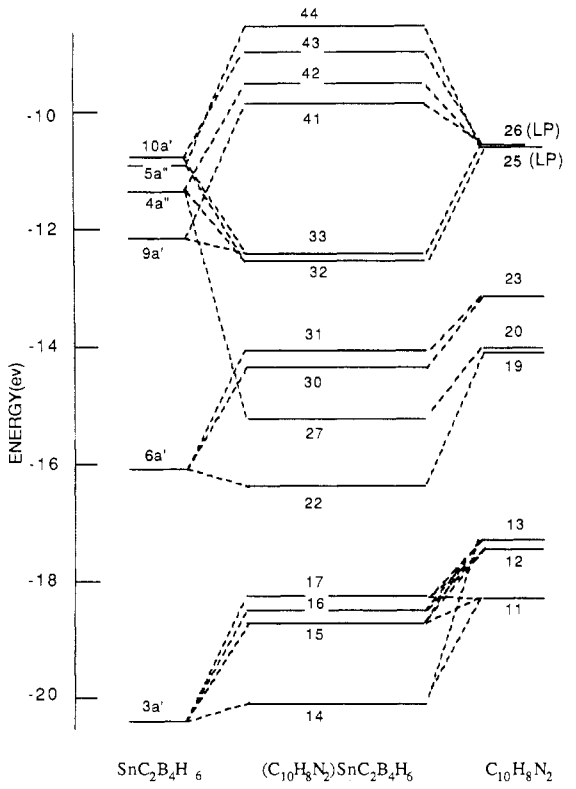

Figure 5. Partial molecular orbital correlation diagram for $(C_{10}H_8N_2)$-$SnC_2B_4H_6$.

of $SnC_2B_4H_6$ shows the same structural change observed experimentally, that is, an increase in the Sn–C_2B_3 distance, an increased slippage of the tin, and the bipyridine molecule directly opposite the cage carbons with a dihedral angle of 22.2°.

The bipyridine molecule has 29 filled MO's while $SnC_2B_4H_6$ has 15. Of the 44 filled MO's in the bipyridine complex, 17 arise from interactions of the tin and the bipyridine. Figure 5 shows a partial molecular orbital correlation diagram for the compound. For simplicity, only those orbitals that strongly interact with tin are shown. The diagram was constructed by tracing the filled molecular orbitals of the complex as the tin–bipyridine distance was increased, using the noncrossing rule, and by inspection of the atomic orbital coefficients. No attempt was made to account for interactions of these orbitals with the virtual orbitals. Barreto and Fehlner[11,40] have made an extensive study of orbital interactions on complexation with bipyridine, and their results will be used in discussing the characteristics of some of the molecular orbitals. In general, when the adduct is formed, all bipyridine orbitals decrease in energy while the carborane orbitals increase. The decrease in bipyridine orbital energies is due to their stabilization by the approach of the positive tin ion, while the increase in carborane energy is the result of the repulsion between the electron-rich carborane and bipyridine fragments. Bipyridine MO's 25 and 26 are heavily localized on the two nitrogen atoms (58% and 62%, respectively) and are directed away from the bipyridine molecule. These constitute the "lone-pair" nitrogen electrons, and they interact strongly with the Sn atom. Several of the adduct MO's are sketched in Figure 6, and their compositions are given in Table 4S of the supplementary material.

MO's 44, 42, 32, and 27. These result from the interaction of $SnC_2B_4H_6$ MO's 4a″ and 5a″ with bipyridine orbitals 25 (lone pair) and 20. The two higher energy MO's, 44 and 42, are carborane based (91% and 99%), resembling 5a″ and 4a″, respectively. The significant change is that MO 42 has essentially no tin character (<0.2%). The two lower energy MO's, 32 and 27, constitute the bonding interactions between the Sn p_z orbital and the bipyridine nitrogens. The important feature of these MO's

(40) Barreto, R. D.; Fehlner, T. P., private communication.

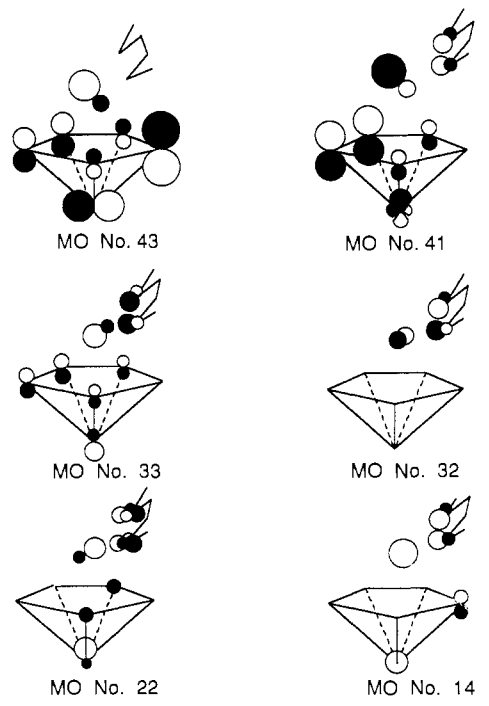

Figure 6. Atomic orbital composition sketches of some molecular orbitals of $(C_{10}H_8N_2)SnC_2B_4H_6$. Only the front end of $C_{10}H_8N_2$ is depicted, and only the nitrogen orbitals are shown.

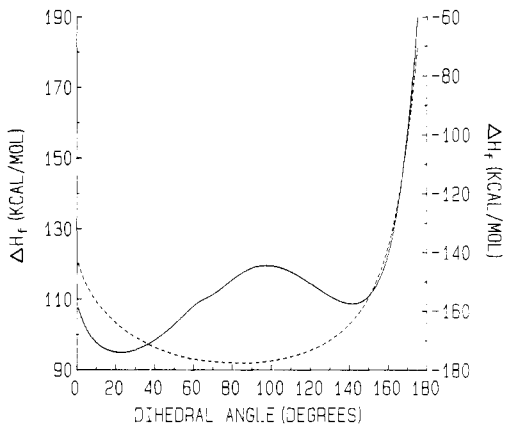

Figure 7. ΔH_f of $(C_{10}H_8N_2)EC_2B_4H_6$ as a function of dihedral angle: solid line, E = Sn, left-hand scale; dashed line, $E = M^{2+}$ (a purely ionic cation), right-hand scale.

is that they contain tin character (4.4% and 1.2%, respectively) but are essentially devoid of carborane character (see Figure 6). The net effect of these interactions is to decrease the extent of Sn p_z bonding to the carborane, especially in 4a″. This would tend to allow greater slippage toward boron.

MO's 43, 41, and 33. These result from the interaction of $SnC_2B_4H_6$ orbitals 10a′ and 9a′ with the symmetric lone-pair bipyridine orbital 26. Molecular orbital 43 is essentially $SnC_2B_4H_6$ MO 10a′ (90%) except that the Sn p_x character has increased (from 5.9% to 12.7%) and the Sn p_y character has decreased (from 17.2% to 6.8%). Molecular orbital 41 is 83% $SnC_2B_4H_6$, similar to 9a′, but has a greater Sn s character and substantially less Sn p_x character (from 10.2% to 3.6%), and the Sn p_y orbital is now antibonding to the cage carbons (see Figure 6). Fenske–Hall calculations by Barreto and Fehlner[40] on the compound (2,2′-bpy)Sn[$C_2(CH_3)_2B_4H_4$] show that the MO corresponding to MO 41 contains, in addition to 9a′ character, about 30% of a base-free virtual orbital where the tin is antibonding to the carborane and about 30% of a nitrogen lone-pair virtual orbital. Although the MNDO program used in this work does not have the fragment basis transformation capability available in Fenske–Hall calculations, MO 41, shown in Figure 6, clearly shows evidence of such

Table IV. One-Center and Two-Center Terms for $(C_{10}H_8N_2)SnC_2B_4H_6$ as a Function of Δ

Δ,[a] Å	−0.538	−0.353	−0.176	0.288	0.633[b]	1.024
$\sum E_{AB}$(cage),[c] eV	−158.842	−159.378	−159.906	−161.194	−161.850	−162.271
$\sum E_{AB}$(Sn−cage), eV	−17.447	−17.559	−17.517	−16.988	−16.482	−16.042
$\sum E_{AB}$(Sn−BP),[d] eV	−4.044	−3.946	−4.084	−4.946	−5.655	−6.223
$\sum E_{AB}$(BP), eV	−345.057	−345.088	−345.092	−345.020	−344.939	−344.836
$\sum E_{AB}$(cage−BP), eV	−0.052	−0.029	−0.045	−0.124	−0.229	−0.338
$\sum E_A$(cage), eV	−454.784	−4549.359	−454.024	−453.477	−453.326	−453.295
E_A(Sn), eV	−83.527	−83.700	−83.758	−83.729	−83.580	−83.402
$\sum E_A$(BP), eV	−1455.462	−1455.539	−1455.467	−1454.811	−1454.297	−1453.886
E, eV	−2519.215	−2519.598	−2519.893	−2520.289	−2520.358	−2520.293

[a] A positive Δ means displacement toward B(4). [b] Optimized value. [c] Cage = $C_2B_4H_6$. [d] BP = 2,2′-bipyridine ($C_{10}H_8N_2$).

high-energy orbital mixing. Molecular orbital 33 is a mixed $SnC_2B_4H_6$ (47%)–bipyridine (53%) MO. It is similar to MO 41 except there is much less cage carbon character and the Sn p_y orbital is bonding to the cage carbons (see Figure 6).

MO's 31, 30 and 22. These MO's arise from the interaction of the $SnC_2B_4H_6$ MO 6a′ with bipyridine orbitals. Since 6a′ is the "lone-pair" orbital, none of these MO's have significant C_2B_3 character. The strongest bonding between tin and bipyridine is in MO 22, which is shown in Figure 6.

MO's 17, 16, 15, and 14. These arise from the interaction of 3a′ with bipyridine MO's 13, 12 and 11. Since 3a′ is localized mainly on B(6) and tin, none of the resulting MO's have significant C_2B_3 character. The strongest tin–bipyridine bonding is in MO 14 (see Figure 6).

Mulliken population analyses of the tin–bipyridine interactions show that the most effective bonding is through the Sn p_y orbital (0.0583) followed by the Sn p_z and Sn p_x orbitals (0.0221 and 0.0150, respectively). As was the case for $SnC_2B_4H_6$, the Sn s orbital is generally antibonding to the bipyridine nitrogens (−0.0542). Table IV lists the one- and two-center terms for the different intramolecular interactions in the system. A comparison of these energies with those of the uncomplexed $SnC_2B_4H_6$, shown in Table III, shows that on complexation, the Sn–cage terms decrease. The decrease in the magnitude of the Sn–cage terms is mainly due to a decrease in E_{Sn-C} of about 50%; $E_{Sn-B(4)}$ decreases slightly and $E_{Sn-B(3/5)}$ increases. The loss in Sn–C bonding is due to MO 41 in which the tin is antibonding to the carbons. Barreto and Fehlner observed this same behavior in the 2,2′-bipyridine–Sn[$C_2(CH_3)_2B_4H_4$] system and attributed the increased slippage of the tin on bipyridine complexation to a relief of the antibonding Sn–C interactions. The present analysis shows that while Sn–C bonding is severely weakened, the overall Sn–C interaction is still bonding as measured by E_{Sn-C}. Other interactions, such as in 1a′, which are not materially perturbed by bipyridine bonding, result in a small Sn–C bonding interaction. Superimposed on tin–cage bonding are the Sn–bipyridine bonding interactions, which increase rapidly as Δ increases. This increased Sn–N bonding and decreased Sn–C bonding gives rise to the increased slip distortion in forming the bipyridine adduct.

As Δ increases, the dihedral angle between the C_2B_3 face of the carborane and the planar rings of the bipyridine decreases, being about 43° at Δ = −0.3 and about 7° at Δ = 1.2. (See Figure 1 for angle definitions.) Mulliken population analyses show that as the dihedral angle decreases, there is an increase in Sn(p_y)–N bonding, a decrease in Sn(p_x)–N bonding while Sn(p_z)–N is unaffected by dihedral angle. Lower dihedral angles also lead to a decrease in Sn s antibonding interactions. (See supplementary Table 5s for overlap populations as a function of dihedral angle.) The decrease in Sn p_x bonding is more than compensated for by the stronger Sn p_y bonding and the decrease in Sn s antibonding interactions. Hence, the most effective tin–bipyridine bonding would occur when the pyridine molecule and the C_2B_3 face were essentially parallel, that is, having a dihedral angle of 0°. Repulsion between the electron-rich bipyridine and $C_2B_4H_6^{2-}$ ligands prevent this favorable orientation. An increased slip distortion of the tin would decrease ligand–ligand repulsion allowing for a lower dihedral angle and hence stronger tin–bipyridine bonding. For metals such as tin that utilize predominately p orbitals in bonding to both the carborane and the Lewis base, ligand–ligand repulsion will be of greater importance than for other metals, such as transition metals, where additional orbitals can be utilized allowing for both maximum bonding and minimum ligand–ligand repulsion. The balance between ligand repulsion and Sn–N bonding is demonstrated in Figure 7, which shows a plot of total energy, measured as ΔH_f of the $(C_{10}H_8N_2)SnC_2B_4H_6$ adduct, as a function of dihedral angle. In these calculations the SnC_2B_4 geometry was held constant as was the tin–bipyridine distance. Also shown in the figure is similar plot when the Sn^{2+} was replaced by a purely ionic +2 ion (M). The plot for $(C_{10}H_8N_2)SnC_2B_4H_6$ exhibits two minima, one at the optimum value of 22.2° and another at about 143°, with a broad maximum at 90°. The $(C_{10}H_8N_2)MC_2B_4H_6$ system shows a single broad minimum at 90°. The sharp increases in energy shown by both systems at the two extremes of 0 and 180° are due to ligand–ligand repulsion. When the tin–bipyridine distance was allowed to vary, calculations showed that, at the extremes, the Sn–N distances increase to the extent that no bond exists. The maximum at 90° for the stannacarborane is due to a decrease in tin–bipyridine bonding as shown in Table IV.

Therefore, one would expect a decrease in dihedral angle and an increase in slip distortion on forming stronger tin–base adducts. The crystal structure of the 2,2′-bipyrimidine complex of *closo*-1-Sn-2,3-$(SiMe_3)_2$-2,3-$C_2B_4H_4$ has recently been reported.[41] The structure shows a smaller slip distortion of the Sn, a larger dihedral angle between the base and the C_2B_3 rings, and longer Sn–N bonds than found in complexes with the more basic bipyridine; all of which are consistent with the above analyses. Jutzi, Cowley, and co-workers have recently reported the structure of the bipyridine complex of 2,3-$(CH_3)_2$-1-Sn-2,3-$C_2B_9H_9$.[42] The same changes occur that are found in the C_2B_4 system, that is, an increased slip distortion with the bipyridine opposite the cage carbons and having a dihedral angle similar to those found in the C_2B_4 system. Since the two carboranes use similar orbitals in bonding to the tin, these results are not unexpected.

When the bipyridine molecule is rotated about the Sn–C_2B_3 axis, the tin moves toward the direction of rotation and the bipyridine molecule twists so that the leading nitrogen is higher above the tin. The leading Sn–N bond distance is now longer than that of the following nitrogen. These distortions are observed in 1-(bpy)-2,3-$(SiMe_3)_2$-1-Ge-2,3-$C_2B_4H_4$.[43]

The position of the tin above the C_2B_3 face in the base–stannacarborane systems will be a function of the strength of the base–tin bond, the number of coordination sites used by the base and the orientation of the base relative to the C_2B_3 atoms. For electron-rich bases such as bipyridine, ligand–ligand repulsion will also be important. These factors are currently under investigation in our laboratories for the stannacarboranes and other main-group metallacarboranes.

Acknowledgment. We thank Southern Methodist University for the use of computer facilities. This work was supported by the National Science Foundation, the Robert A. Welch Foun-

(41) Hosmane, N. S.; Islam, M. S.; Siriwardane, U.; Maguire, J. A.; Campana, C. F. *Organometallics* **1987**, *6*, 2447.
(42) Jutzi, P.; Galow, P.; Abu-Orabi, S.; Arif, A. M.; Cowley, A. H.; Norman, N. C. *Organometallics* **1987**, *6*, 1024.
(43) Hosmane, N. S.; Siriwardane, U.; Islam, M. S.; Maguire, J. A.; Chu, S. S. C. *Inorg. Chem.* **1987**, *21*, 3428.

dation, and the donors of the Petroleum Research Fund, administered by the American Chemical Society.

Supplementary Material Available: Heavy-atom compositions of the molecular orbitals of $C_2B_4H_6^{2-}$ (Table 1S), composition of molecular orbitals of $SnC_2B_4H_6$ (Table 2S), calculated Mulliken charges and Δ for substituents on $SnC_2B_4H_3R_3$ (Table 3S), composition of the molecular orbitals of $(C_{10}H_8N_2)SnC_2B_4H_6$ (Table 4S), and Mulliken overlap populations for $(C_{10}H_8N_2)SnC_2B_4H_6$ (Table 5S) (5 pages). Ordering information is given on any current masthead page.

Contribution from the Department of Biochemistry and Molecular Biology, Cummings Life Science Center, The University of Chicago, 920 East 58th Street, Chicago, Illinois 60637

ENDOR-Determined Solvation Structure of VO^{2+} in Frozen Solutions[1]

Devkumar Mustafi and Marvin W. Makinen*

Received October 16, 1987

The solvation structure of the vanadyl ion (VO^{2+}) in methanol and in water-methanol mixtures has been investigated by application of ^1H and ^{13}C electron nuclear double resonance (ENDOR) spectroscopy. The ligand origins of the proton ENDOR resonances have been assigned with use of materials selectively enriched with ^2H. The principal hyperfine coupling (hfc) components of both ^1H and ^{13}C in solvent molecules coordinated to the VO^{2+} ion have been determined by analysis of the $\mathbf{H}_0$ dependence of the ENDOR spectra. The hfc components of ^1H and ^{13}C of both metal-bound water and methanol exhibit axial symmetry. Under the point-dipole approximation the anisotropic hfc components yield estimates of the separation between the paramagnetic center and the ^1H and ^{13}C nuclei of axially and equatorially bound solvent molecules. Axially coordinated H_2O molecules exhiibit metal-proton distances of 2.92 and 3.42 Å, respectively, corresponding to an inner-sphere coordination site on one side of the equatorial plane and to a site with hydrogen bonding to the V=O group on the other side. Equatorially coordinated H_2O molecules exhibit metal-proton distances of 2.60 and 4.80 Å, corresponding to an inner-sphere coordination site and a hydrogen-bonded outer-sphere coordination site. In pure methanol there are similarly inner-sphere- and outer-sphere-bound methanol molecules in equatorial and axial positions, and the coordination structure determined on the basis of the metal-proton distances is confirmed by ENDOR spectroscopy with ^{13}C-enriched methanol. The ENDOR results provide unambiguous evidence that in water-methanol mixtures only $VO(H_2O)_5^{2+}$ and $[VO(H_2O)_4(CH_3OH)]^{2+}$ species are formed. In pure methanol the $VO(CH_3OH)_5^{2+}$ species is observed. The coordination geometries of the VO^{2+} complexes are deduced from ENDOR estimates of metal-nucleus distances by using computer-based molecular graphics. It is shown on the basis of molecular modeling that the ENDOR-determined metal-nucleus distances are best accounted for by complexes of tetragonal-pyramidal geometry.

Introduction

Complexes of the vanadyl ion (VO^{2+}) are stable and magnetically well-behaved and have been employed widely in spectroscopic studies. Although it is generally accepted that the VO^{2+} ion exists as a pentaaquo-hydrated species in solution, the actual composition of the complex has not been demonstrated. The structure of the $VO(H_2O)_5^{2+}$ species was first formulated for the complex in aqueous solution on the basis of its electronic absorption spectrum,[2] modeled according to the square-pyramidal geometry of the pentacoordinate complex of VO^{2+} with acetylacetonate[3] and of $VO(H_2O)_4(SO_4)\cdot H_2O$ in crystals.[4] While nuclear magnetic resonance studies with use of oxygen-17-enriched water identified dipolar interactions within the complex of the solvated VO^{2+} ion that could be ascribed to equatorial $V\cdots OH_2$ interactions,[5] dipolar couplings could not be unambiguously assigned to an axial H_2O molecule.[6] Furthermore, the original X-ray study of $VO(H_2O)_4SO_4\cdot H_2O$ was analyzed only on the basis of Patterson projections[4,7] and the completed refinement of the crystallographic parameters determined in the subsequent study of Ballhausen, Djurinskij, and Watson[8] has not been reported. The structure analysis, thus, remains incomplete. Moreover, the $VO(H_2O)_5^{2+}$ species has not been observed hitherto in any crystal environment.

Since the first demonstration of electron nuclear double resonance[9] (ENDOR[10]), it has been used widely to characterize paramagnetic sites in solids and liquids. The electron spin of the paramagnetic site interacts with magnetic nuclei in its nearby environment through dipolar and contact interactions, producing shifts in their resonance frequencies. The dipolar interaction depends on the relative position of the nuclear spin with respect to the unpaired spin. ENDOR spectra of solid samples, obtained by partially saturating an EPR transition and sweeping a radio-frequency field through nuclear resonance transitions, can be analyzed to yield the dipolar contributions and to determine nuclear coordinates. Application of the theoretical equations relating the magnetic couplings of the **g** matrix and the hf interaction matrix to the set of molecular orientations selected for nuclear resonance in an ENDOR experiment becomes particularly straightforward in the case of paramagnetic sites of low g anisotropy,[11] as is the case for the VO^{2+} ion. We have employed ENDOR spectroscopy to determine the coordination environment of the Gd^{3+} ion[12] and to assign the conformation of nitroxyl

(1) This work was supported by grants from the National Institutes of Health (GM 21900 and AA 06374).
(2) Ballhausen, C. J.; Gray, H. B. *Inorg. Chem.* **1962**, *1*, 111-122.
(3) Dodge, R. P.; Templeton, D. H.; Zalkin, A. *J. Chem. Phys.* **1961**, *35*, 55-67.
(4) Palma-Vittorelli, M. B.; Palma, M. U.; Palumbo, D.; Sgarlata, F. *Nuovo Cimento* **1956**, *3*, 718-730.
(5) (a) Wüthrich, K.; Connick, R. E. *Inorg. Chem.* **1967**, *6*, 583-590. (b) Reuben, J.; Fiat, D. *Inorg. Chem.* **1969**, *8*, 1821-1824.
(6) Reuben, J.; Fiat, D. *Inorg. Chem.* **1967**, *6*, 579-583.
(7) The use of computers in reduction and full-matrix least-squares refinement of X-ray data was not then common practice. Thus, although the coordination structure deduced by Palma-Vittorelli et al.[4] yields distorted bonding relationships, it cannot be considered as erroneous without least-squares refinement of the atomic coordinates and temperature factors derived from the X-ray intensity data.
(8) Ballhausen, C. J.; Djurinskij, B. F.; Watson, K. J. *J. Am. Chem. Soc.* **1968**, *90*, 3305-3309.
(9) (a) Feher, G. *Phys. Rev.* **1956**, *103*, 834-835. (b) Feher, G. *Phys. Rev.* **1959**, *114*, 1219-1244.
(10) The following abbreviations are used: ENDOR, electron nuclear double resonance; EPR, electron paramagnetic resonance; hf, hyperfine; hfc, hyperfine coupling; rf, radio frequency.
(11) (a) Hurst, G. C.; Henderson, T. A.; Kreilick, R. W. *J. Am. Chem. Soc.* **1985**, *107*, 7294-7299. (b) Henderson, T. A.; Hurst, G. C.; Kreilick, R. W. *J. Am. Chem. Soc.* **1985**, *107*, 7299-7303.
(12) (a) Yim, M. B.; Kuo, L. E.; Makinen, M. W. *J. Magn. Reson.* **1982**, *46*, 247-256. (b) Yim, M. B.; Makinen, M. W. *J. Magn. Reson.* **1986**, *70*, 89-105.

0020-1669/88/1327-3360$01.50/0 © 1988 American Chemical Society